Fuel 276 (2020) 118032

Contents lists available at ScienceDirect

Fuel

journal homepage: www.elsevier.com/locate/fuel

Full Length Article

Tuning amphiphilic properties of Ni/Carbon nanotubes functionalized catalysts and their effect as emulsion stabilizer for biomass-derived furfural upgrading

C. Herrera[a,b], L. Barrientos[a,b,c], A. Rosenkranz[d], C. Sepulveda[b,e], J.L. García-Fierro[f], M.A. Laguna-Bercero[g], N. Escalona[a,b,c,h,i,*]

[a] Facultad de Química y Farmacia, Pontificia Universidad Católica de Chile, Santiago, Chile
[b] Millenium Nuclei on Catalytic Processes Towards Sustainable Chemistry (CSC), Chile
[c] Centro de Investigación en Nanotecnología y Materiales CIEN-UC, Pontificia Universidad Católica de Chile, Chile
[d] Facultad de Ciencias Físicas y Matemáticas, Departamento de Ingeniería Química, Biotecnología y Materiales, Universidad de Chile, Santiago, Chile
[e] Facultad de Ciencias Químicas, Universidad de Concepción, Casilla 160C, Chile
[f] Instituto de Catálisis y Petroleoquímica CSIC, Cantoblanco, Madrid, Spain
[g] Instituto de Ciencia de Materiales de Aragón, ICMA, CSIC-Universidad de Zaragoza, María de Luna 3, 50018 Zaragoza, Spain
[h] Departamento de Ingeniería Química y Bioprocesos, Escuela de Ingeniería, Pontificia Universidad Católica de Chile. Avenida Vicuña Mackenna 4860, Macul, Santiago, Chile
[i] Unidad de Desarrollo Tecnológico, Universidad de Concepción, Coronel, Chile

GRAPHICAL ABSTRACT

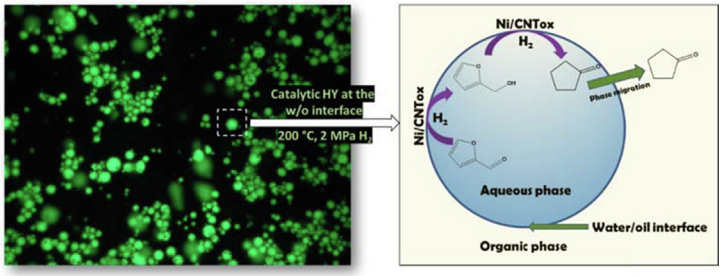

ARTICLE INFO

Keywords:
Emulsion
Furfural
Hydrogenation
Cyclopentanone
Biomass
Carbon nanotubes

ABSTRACT

Three amphiphilic carbon nanotube-supported Ni catalysts have been prepared and tested regarding their emulsifying properties for the hydrogenation of furfural. The solid catalysts and emulsions were systematically characterized by different high-resolution techniques. The catalytic hydrogenation of furfural was evaluated in a mixture of two immiscible solvents under mild conditions. The wettability of the catalysts was tuned by adjusting the severity of the acid treatments during the catalyst's synthesis. It was found that the catalysts wettability played a crucial role in enhancing the catalytic activity. The lowest furfural conversion observed over Ni/$CNTox_2$ and Ni/CNTp were attributed to the missing possibility to form stable emulsion droplets due to their either extreme hydrophilic or hydrophobic character, respectively. In contrast, the highest catalytic activity verified for Ni/$CNTox_1$ catalyst was traced back to an improved dispersion of the nickel nanoparticles as well as the possible formation of stable emulsion droplets due to its amphiphilic character. All catalysts were selective towards cyclopentanone. However, the highest yield of cyclopentanone was found over the Ni/$CNTox_1$ catalyst,

* Corresponding author at: Escuela de Ingeniería, Pontificia Universidad Católica de Chile, Santiago, Chile.
E-mail address: neescalona@ing.puc.cl (N. Escalona).

https://doi.org/10.1016/j.fuel.2020.118032
Received 10 March 2020; Received in revised form 3 May 2020; Accepted 5 May 2020
Available online 20 May 2020
0016-2361/

which migrated towards the organic phase after its formation. This result highlights the simultaneous reaction and separation of key reaction products in emulsion, which greatly simplifies the isolation stages of target products.

1. Introduction

The conversion of lignocellulosic biomass to biofuel and add-value chemicals is one of the most promising routes to decrease the dependency on fossil fuels thus potentially reducing greenhouse emissions [1,2]. Derived from pyrolysis of renewable biomass, bio-oil is a complex liquid, which is only partially soluble in either water or hydrocarbon solvents. It contains more than 400 organics compounds such as phenols, guaiacols, furan and their derivatives [3,4]. Due to the unstable composition of bio-oil, an upgrading process is required to improve their fuel properties and to obtain add-value chemicals [5]. Among several strategies, catalytic hydrogenation (HY) is considered as a promising route for bio-oil upgrading [6,7]. It has been reported that a wide range of biomass derivates such as phenol, sorbitol, anisol and furfural can be hydrogenated to obtain liquid fuels for the transportation sector. In this regard, catalytic conversion of furfural represents one of the most important routes for the production of fuel additives, high value-added chemicals and biofuels [8]. Several research papers have been published in the past decade dealing with homogeneous and heterogeneous catalytic processes to upgrade furfural to relevant drop-in fuel candidates (such as 2,5-dimethylfuran (DMF) and 2-methylfuran (2-MF)) and value-added chemicals such as furfuryl alcohol (FUR-OH), levulinic acid (LA) and cyclopentanone (CPO) [9,10]. A summary of previous studies regarding the catalytic conversion of furfural over heterogeneous catalysts can be found in Table S1 (supplementary information). Special attention has been laid on studies reporting on the formation of cyclopentanone and cyclopentanol. These studies include the usage of different catalysts based upon noble metals [11–14] and non-noble metals [10,15]. Cyclopentanone is a versatile compound used for the synthesis of fungicides, pharmaceuticals, rubber chemicals, and flavoured fragrance chemicals [16]. It can be potentially used for the preparation of polyamides, C_{15}-C_{17} diesel or jet fuels and polyolefin stabilizers [17].

Liquid phase conversion of furfural has been only studied over a variety of catalysts in monophasic systems [18,19]. Catalytic conversion in single-phase hinder the separation of target products from the reaction medium thus transforming them in undesired intermediaries' reactions. Moreover, in case of refining bio-oils for which the system is a biphasic mixture of water (30%) and non-polar molecules, the most efficient way to catalyze a reaction is to disperse an amphiphilic catalyst at the liquid/liquid interface and maximize the interfaces extent by forming stable emulsion droplets [20]. Therefore, the catalytic transformation of biomass and its derived compound (such as furfural) toward value-added chemicals requires the development of new proper catalysts that are capable to act as both emulsifiers and catalysts.

Recently, it has been proven that solid particles with amphiphilic character can be utilized to stabilize water–oil emulsions (Pickering emulsions) [21]. In literature, it has been reported that different parameters such as the hydrophilic/hydrophobic character, droplet size, amphiphilic solid concentration, pH reaction medium and sonication time can affect the resulting emulsion properties. For instance, the average droplet size decreases with sonication time and amphiphilic particles' concentration, thus improving the emulsion stability [22]. The main characteristic of the amphiphilic catalysts is their ability to enhance the liquid–liquid interfacial area, which facilitates the simple separation of molecules based upon solubility differences [23]. One strategy used to synthesize an amphiphilic material is surface functionalization. It has been shown that faujasite HY zeolites tend to become hydrophobic by functionalization with organosilanes thus enabling the zeolites to stabilize water/oil emulsions and catalyze reactions of importance in biofuel upgrading, i.e., alkylation of m-cresol and 2-propanol in the liquid phase at high temperatures [24]. Another approach to elaborate a nanohybrid catalyst is the fusion of two solids with opposite properties. Crossley *et al.* synthesized an amphiphilic material consisting of hydrophobic carbon nanotubes fused to hydrophilic metal oxide (silica). They found that these materials had a remarkably high affinity to the liquid–liquid interface, which allowed them to stabilize emulsions with small droplet sizes [22]. Moreover, by incorporation of Pd nanoparticles to the nanohybrids, the authors reported their application in the hydrodeoxygenation (HDO) of vanillin [25]. Nevertheless, despite of the positive results reported in biomass-derived conversion, the use of theses nanohybrids as emulsion stabilizer and catalysts has been limited to hydrogenation of vanillin (biomass-derived polyol compounds) [26,27] and C–C coupling reactions (such as aldol-condensation and alkylation reaction) [28,29]. There is no report available dealing with the application of amphiphilic catalysts in the conversion of furfural (biomass-derived furanic compounds) in emulsion systems.

The conducted literature review indicates that the catalysts' wettability plays an important role in the conversion of bio-oil model molecules and needs be designed carefully to obtain a desirable catalytic performance. Different carbon materials such as carbonaceous microspheres, functionalized graphene and graphene oxide have been reported as effective emulsifiers due to the possibility to chemically functionalized them. Furthermore, these materials can be decorated with metallic nanoparticles (NPs) to enable novel catalytic activity [26,30]. It is well known that carbon nanotubes (CNT) exhibit several promising features as catalytic support due to their surface reactivity and chemical tunability achieved by functionalization [31]. Moreover, different functionalization parameters such as temperature, time, concentration and oxidizing agent can be adjusted to modify their surface properties and wettability [32,33]. In this work, the chemical oxidation of CNTs by two reagents that possess different degrees of oxidation power was studied to reduce the hydrophobic character of the nanotubes. Then, their amphiphilic properties and ability to be used as emulsifier were investigated. Additionally, by doping the as-functionalized CNTs with Ni nanoparticles, their catalytic behavior in the hydrogenation of furfural, as a model biomass-derived upgrading reaction, in biphasic medium was studied. The optimum experimental functionalization conditions for the formation of a stable emulsions has been derived, which can be used as a guide for further materials functionalization in this context in the future.

2. Experimental

2.1. Synthesis of the catalysts

The Ni-based catalysts were supported over CNTs with different degrees of surface functionalization. Prior to usage, 1.0 g of pristine CNT (CNTp) was oxidized with 10.0 mL of HNO_3 solution (65%, Merck) during 24 h at 130 °C under stirring (denominated $CNTox_1$). Furthermore, 3.0 g of CNTp was refluxed in a mixture of HNO_3 (68%, 168.75 mL, Merck) and H_2SO_4 (97%, 56.25 mL, Merck) at 130 °C for 24 h under stirring (denominated $CNTox_2$). Then, the solids were filtered and washed with deionized water until reaching a neutral pH. Finally, the supports were dried at 110 °C for 12 h. The nanohybrid Ni/CNTs catalysts were prepared by incipient impregnation of an aqueous solution of nickel (II) nitrate hexahydrate (≥99%, $Ni(NO_3)_2{\cdot}6H_2O$, Merck) with 10 wt% Ni over CNTp, $CNTox_1$ and $CNTox_2$ supports. The catalysts were then dried overnight at 110 °C and calcined in air for 1 h

at 300 °C. Finally, the catalysts were reduced in H_2 flow (60.0 mL min^{-1}) for 4 h at 400 °C and passivated in 1% O_2/N_2 flow (60.0 mL min^{-1}) for 1 h with the reactor immersed in liquid nitrogen/isopropanol bath, and then passivated for an additional 1.5 h at room temperature. The obtained catalysts were denominated as Ni/CNTp, $Ni/CNTox_1$ and $Ni/CNTox_2$.

2.2. Catalysts characterization

Temperature-programmed decomposition (He-TPD/MS) of CNT supports and Ni/CNTs catalysts was carried out using a Micromeritics 3Flex equipment. In each experiment, 0.035 g of sample were heated up to 800 °C with a rate of 10 °C min −1 under a constant helium flow of 100 mL min^{-1}. The acidity of the Ni/CNTs catalysts was determined by temperature-programmed desorption of ammonia (TPD-NH_3) using the same apparatus. The sample was first dried under He (50 mL min^{-1}) at 110 °C for 30 min, reduced under H_2 (50 mL min^{-1}) at 400 °C for 4 h, and cooled to 110 °C under He. The sample was then saturated with NH_3 using He (50 mL min^{-1}) as a carrier gas, purged with He for 0.5 h to remove physisorbed NH_3, and, subsequently, cooled to ambient temperature under He. Once the TCD baseline was restored, NH_3-TPD was performed at a heating rate of 10 °C min^{-1} up to 80 °C in flowing He (50 mL min^{-1}). BET Surface area (S_{BET}) and textural properties of CNT supports, and Ni/CNT-based catalysts were determined by N_2 physisorption at −196 °C using a Micromeritics 3Flex equipment. Temperature-programmed reduction (H_2-TPR) were obtained using a Micromeritics 3Flex equipment with a thermal conductivity detector. In each experiment, 0.035 g of the sample was heated under 5% H_2/Ar with a flow of 100 mL min^{-1}. The sample was heated up to 1050 °C at a rate of 10 °C min^{-1}. High-resolution transmission electron microscopy (HR-TEM) was performed using a JEOL 2000FX TEM microscope at 200 kV to characterize the average particle size, distribution and microstructure of the reduced-passivated Ni/CNTs catalysts. The average particle size was calculated using the DigitalMicrograph by analyzing more than 300 individual particles. Metal dispersion was estimated from CO chemisorption using a Micromeritics 3Flex apparatus. The catalysts (0.05 g) were reduced *in-situ* under H_2 flow during 4 h at 400 °C. Ni dispersion was calculated by assuming a CO:Ni stoichiometry of 1:1. X-ray photoelectron spectroscopy (XPS) of in-situ reduced catalysts were recorded on a VG Escalab 200R electron spectrometer using a Mg Kα (1253.6 eV) photon source. The binding energies (BE) were referenced to the C_{1s} level of the carbon support at 284.8 eV. An estimated error of ± 0.1 eV can be assumed for all measurements. The intensities of the peaks were calculated from the respective peak areas after background subtraction and spectrum fitting by the standard computer-based statistical analysis, which included fitting the experimental spectra. The wettability of the catalysts was investigated by measuring the static contact angles (θ) with distilled water (volume of 2 μL). The static contact angles were measured under ambient conditions using a self-supporting pressed sample (drop shape analyzer DSA-25-E, Krüss GmbH). The optical/fluorescent micrograph was obtained in an Axiostar plus Carl Zeiss microscope equipped with an HBO 50 mercury vapor lamp.

2.3. Preparation of emulsion using different nanohybrid catalysts

To prepare the water/oil emulsion with different nanohybrid catalysts, deionized water and dodecane were used as aqueous and organic phases, respectively. In each experiment, 50 mg of catalyst was initially dispersed in the water phase (25 mL) by sonication with a horn sonicator (UP50H, Hielscher) at 25% of amplitude for 15 min. Subsequently, 25 mL of dodecane volume was added (water:dodecane ratio equal to 1:1) and the final mixture was sonicated at 50% of amplitude for 15 min.

2.4. Hydrogenation of furfural

The hydrogenation reaction was carried out in a Batch Parr 4561 reactor. In each experiment, 0.232 mol L^{-1} of furfural was added to the sonicated mixture of water, dodecane and catalyst. Prior to reaction, the vessel reactor was purged with N_2 flow during 15 min to remove the oxygen content inside of the reactor. Then, the reactor was heated up under speed stirred (500 rpm) to the reaction temperature (200 °C) and the H_2 pressure was adjusted (2.0 MPa). After each reaction, the reactor was cooled down and the H_2 flow was replaced by N_2 flow. Once the reactor had reached room temperature, the emulsion was broken by filtering out the catalyst. The liquid phases were separated and analyzed individually by GC with flame-ionization detector (FID) and an Elite-1 column (Perkin Elmer, 30 m × 0.53 mm × 3.0 μm film thickness). The products were also identified by their column retention time compared to available standards. The carbon mass balance was estimated as the sum of the yields of products determined and unconverted furfural. According to this, all catalysts show a mass balance over 90%. Conversion of furfural and selectivity are defined as follows:

$$conversion\ of\ FAL = \frac{moles\ of\ FAL\ reacted}{moles\ of\ FAL\ initial} \text{x100} \quad (1)$$

$$(Yield\ of\ product)_i = \frac{(moles\ of\ product)_i}{moles\ of\ FAL\ initial} \text{x100} \quad (2)$$

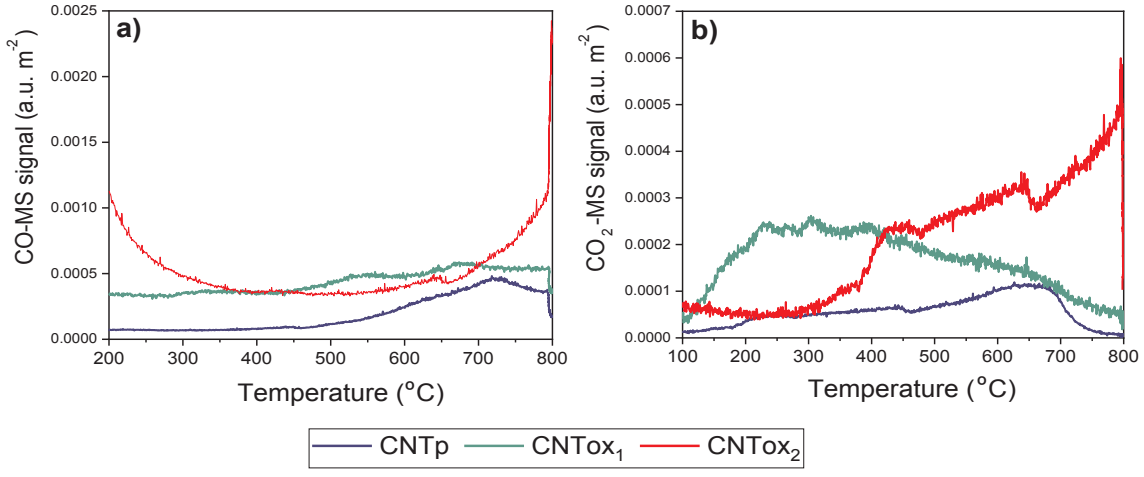

Fig. 1. He-TPD/MS profile of pristine and modified CNT samples, a) CO-MS and b) CO_2-MS signals.

3. Results and discussion

3.1. Characterization of the catalysts

The He-TPD/MS profiles of the pristine and oxidized CNTs are shown in Fig. 1. The CO signal evolution (Fig. 1a) of the untreated CNTp displays a broad band in the range of intermediate/high temperatures (550–800 °C), whereas the oxidized $CNTox_1$ shows two overlapping bands at intermediate (450–600 °C) and high decomposition temperatures (600–750 °C). In contrast, the oxidized $CNTox_2$ only reveals an increased signal at high temperatures (700–800 °C). According to previously published work [32,33], these peaks typically arise from the decomposition of carboxylic anhydrides (527–677 °C), phenols/ethers (677–727 °C) and carbonyls/quinones (800–877 °C) groups [34,35]. Moreover, the evolution of CO_2 signal (Fig. 1b) of the untreated CNTp displays a broad band at intermediate (450–750 °C) decomposition temperatures, while the $CNTox_1$ sample demostrates a broad band over the entire temperature range (between 200 and 750 °C). Moreover, the more intensely oxidized $CNTox_2$ support presents two peaks at low (300–380 °C) and intermediate temperatures (400–650 °C) and a signal increase at high decomposition temperatures (650–800 °C). The peaks appearing in the CO_2-MS profile can be assigned to carboxylic acids (peaks below 450 °C), carboxylic anhydrides (between 527 and 677 °C) and lactones (627–827 °C) [33]. These results demonstrate the effective formation of surface oxygen groups over functionalized $CNTox_1$ and $CNTox_2$ supports during both nitric acid and acid mixture treatments. However, the last process produces the highest concentration of surface oxygen groups, thus leading to a release of larger amounts of CO and CO_2.

The TPD-MS profiles of the CNT-supported Ni catalysts provide valuable information on the influence of the surface oxygen groups on nickel grafting. The CO-MS and CO_2-MS profiles of the Ni/CNTs catalysts are displayed in Fig. 2a and b, respectively. The CO-MS evolution (Fig. 2a) of the Ni/CNTp displays a narrow peak at 452 °C, whereas the $Ni/CNTox_1$ catalyst shows a narrow peak in the range of intermediate decomposition temperature around 487 °C. In contrast, $Ni/CNTox_2$ displays two narrow peaks at 426 and 541 °C. The presence of theses peaks indicates that the nickel incorporation (and subsequence reduction) over these three supports modified the composition of oxygen-containing surface groups, favoring a narrow distribution in the region of carboxylic anhydride groups [36]. Furthermore, Fig. 2a shows that after the incorporation of Ni on CNTp, $CNTox_1$ and $CNTox_2$ supports, no signs of decomposition of surface oxygen groups high temperatures (650–900 °C), such as phenols/ethers and carbonyl groups are observed. In Fig. 2b, the CO_2-MS profile demonstrates that Ni/CNTp catalyst presents a narrow peak at 448 °C, while the $Ni/CNTox_1$ catalyst displays a narrow peak at 484 °C. In the case of the $Ni/CNTox_2$, two peaks appeared at 261 and 414 °C. These observations suggest that the incorporation of Ni on CNTp, $CNTox_1$ and $CNTox_2$ produces a narrow distribution of surface oxygen groups (such as carboxylic anhydride) that release CO_2 at intermediate temperatures. Furthermore, the additional decomposition peak observed at lower temperature (261 °C) over $Ni/CNTox_2$ catalyst points towards the presence of carboxylic acids. Moreover, for all Ni/CNTs catalysts, the surface oxygen groups that release CO_2 in the temperature range of 550–900 °C disappear after Ni metal deposition. A similar behavior was reported by Machado *et al.* [33] over Ru/CNTs catalysts. These authors observed that the ruthenium deposition on CNTox surfaces led to the disappearance of most of the carboxylic acid (peak at 292 °C), anhydride (peak at 462 °C), and lactone groups (peak at 677 °C) inducing the formation of new CO_2 releasing groups. Furthermore, under experimental conditions of Ni reduction, surface oxygen groups could be reduced to a certain extent.

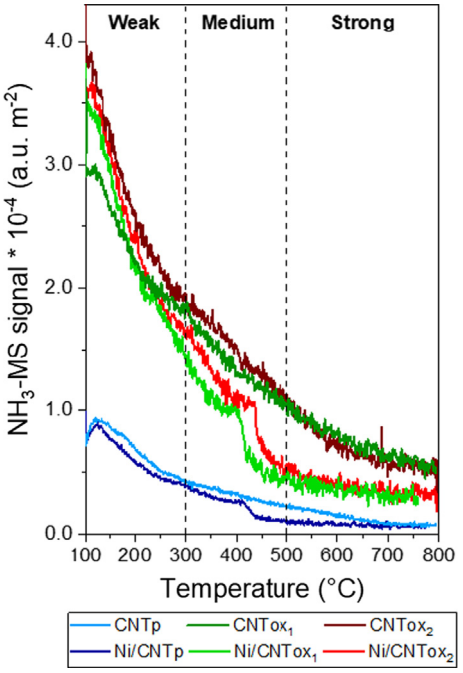

Fig. 3. NH_3-MS profiles of CNTs supports and CNT-supported Ni nanohybrid catalysts.

Temperature-programmed desorption of ammonia (NH_3-TPD/MS) were conducted to evaluate the acidity of the CNTs supports and the CNT-supported Ni catalysts. The corresponding profiles are depicted in Fig. 3. Although ammonia desorption does not allow to discriminate between Brønsted and Lewis acid sites, the amount of desorbed NH_3 is an indirect measure of the material overall acidity. According to previous reports, the strength of the acid sites can be classified as weak

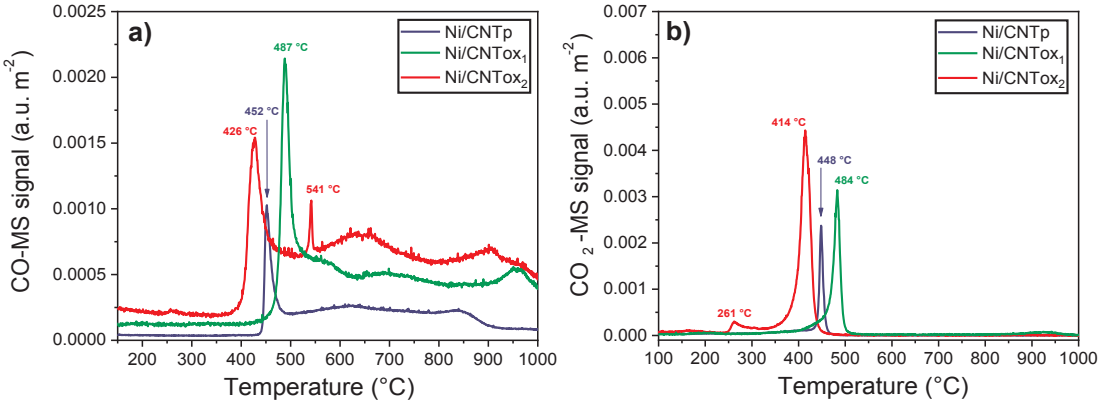

Fig. 2. He-TPD/MS profile of CNT-supported Ni catalysts, a) CO-MS signal and b) CO_2-MS signal.

acid sites (T < 300 °C), medium acid sites (300 °C < T < 500 °C) and strong acid sites (T greater than 500 °C) [37]. As can be seen in Fig. 3, the ammonia amounts desorbed decrease in the following order $CNTox_2$ > $Ni/CNTox_2$ > $CNTox_1$ > $Ni/CNTox_1$ > CNTp > Ni/CNTp. This trend indicates that an increase of oxidation severity results in an increase of the surface acid sites density, which can be related to the generation of surface oxygen groups, which is in good agreement with He- TPD/MS results. Furthermore, the comparison of ammonia desorbed profiles between each supports and their respective CNT-supported Ni catalysts (e.g. CNTp and Ni/CNTp) shows that the amount of ammonia desorbed decrease after Ni incorporation. This implies that the Ni nanoparticles were anchored and dispersed over the surface oxygen groups. In terms of acid strength, all Ni/CNTs catalysts profiles show ammonia desorption mainly in the lower-intermediate temperature range thus indicating the presence of weak and medium acid sites. However, it is worth pointing out that the $Ni/CNTox_2$ displayed the highest density of medium acid sites. This result suggests that acid mixture treatment favors the formation of medium acid sites rather than the formation of weak acid sites, which are promoted by nitric acid treatment.

Fig. 4a shows the N_2 adsorption–desorption isotherms at −196 °C of the calcined and oxidized CNTs. It can be observed that the CNTp support exhibits a type IV isotherm, typical for mesoporous materials, while the $CNTox_1$ and $CNTox_2$ supports display a type II isotherm, being typical for macroporous solids according to the IUPAC classification [38]. Additionally, their BJH plots are shown in Fig. 4a (inset in

Table 1
Textural properties of CNTs support and calcined Ni/CNT-functionalized catalysts measured by N_2 physisorption.

Catalysts	S_{BET}	S^*_{BET} [a]	V_p [b]	d_p [c]
	($m^2\ g^{-1}$)	($m^2\ g^{-1}$)	($cm^3\ g^{-1}$)	(nm)
CNTp	634	–	0.98	11
Ni/CNTp	550	571	0.88	14
$CNTox_1$	115	–	1.06	62
$Ni/CNTox_1$	119	104	0.75	57
$CNTox_2$	126	–	1.05	58
$Ni/CNTox_2$	119	113	0.91	63

[a] Theoretical specific surface area calculated based upon support contribution (S_{BET} value of CNTs support).
[b] Recorded at a relative pressure of 0.96.
[c] Estimated by 4 V/A from BET, where V refers to total pore volume and A to surface area, respectively.

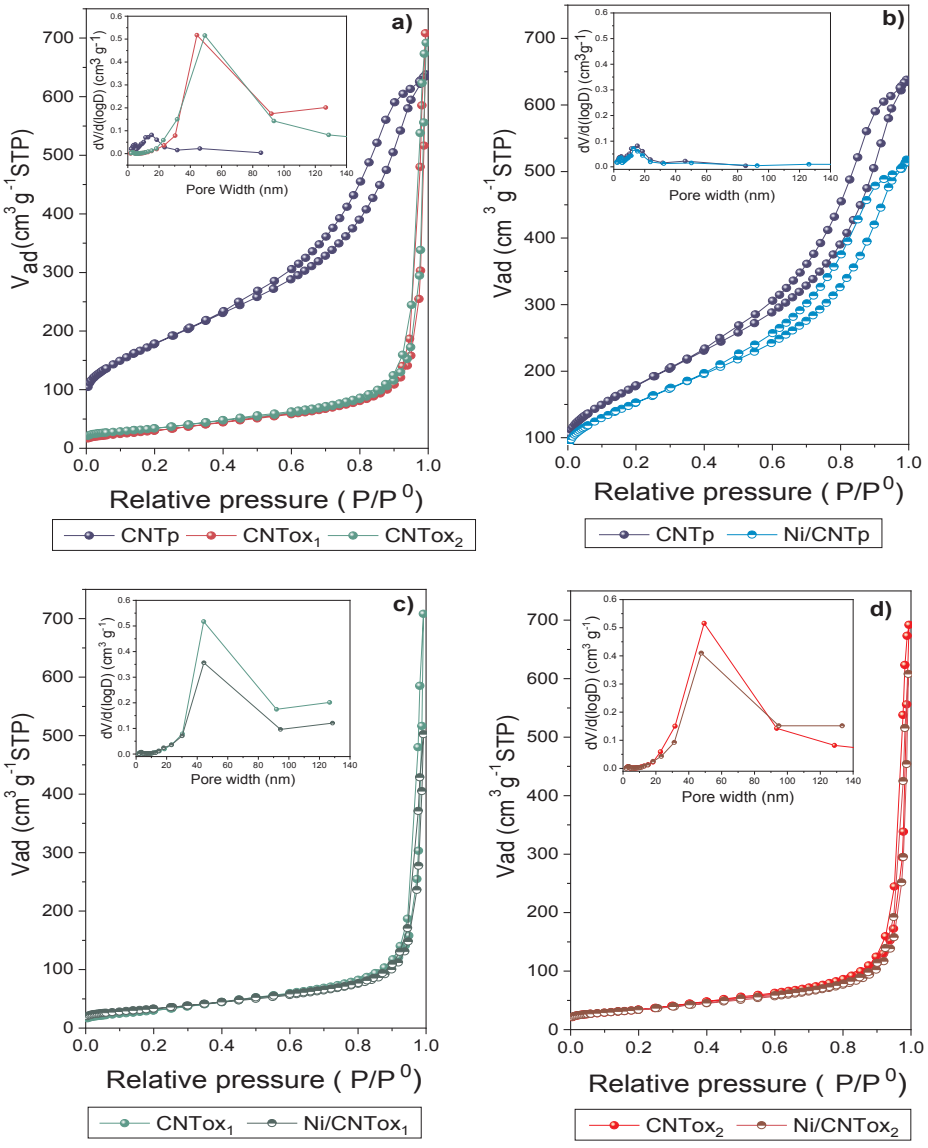

Fig. 4. N_2 physisorption isotherms and BJH calculations (inset) for a) calcined CNT supports; b) Ni/CNTp; c) $Ni/CNTox_1$ and d) $Ni/CNTox_2$ catalysts.

the graphs). In these insets, the CNTp support demonstrate an average pore diameter centered at 11 nm corresponding to mesoporous structures, whereas the $CNTox_1$ and $CNTox_2$ supports display an increased average pore diameter of 62 and 58 nm, respectively. These results suggest that these acid-functionalization treatments favor the formation of macroporous structures thus destroying the initial mesoporous structure [36]. Fig. 4b-d show the N_2 adsorption–desorption isotherms of the Ni-supported catalysts. After the deposition of Ni nanoparticles over the CNTs, the type of the isotherm and the amount of N_2 adsorbed have not been modified. The surface area (S_{BET}), theoretical surface area (S^*_{BET}), total pore volume (V_p), mesoporous volume (V_m) and pore diameter (d_p) of the supports and calcined Ni/CNTp, $Ni/CNTox_1$ and $Ni/CNTox_2$ catalysts are summarized in Table 1. It can be seen that the BET surface area significantly decreased after oxidation with both nitric acid and acid mixtures. However, it has been reported that impregnation with concentrate HNO_3 for 4 h slightly increased the surface area of multi-wall CNTs due to CNT tip opening [33]. Therefore, long impregnation times (24 h) with HNO_3 induce a loss of the graphitic structure thus decreasing S_{BET}. Additionally, CNT tip opening can not be ruled out. The comparison of S_{BET} with the S^*_{BET} values of Ni/CNTp, $Ni/CNTox_1$ and $Ni/CNTox_2$ (Table 1) shows similar surface area values (considering an error of 10–15% in S_{BET}), thus suggesting no pore blockage.

H_2-TPR profiles of the Ni/CNT-functionalized catalysts are shown in Fig. 5. All Ni-based catalysts show a reduction peak at 380 °C and a broad band at a higher reduction temperature centered at 487 °C. An additional reduction peak at 291 °C has been observed for $Ni/CNTox_1$ and $Ni/CNTox_2$ catalysts. According to a previous study [39], it has been reported that the nature of the support used and the synthesis conditions affect the reducibility of the Ni species. Suhong *et al.* reported that for nickel supported CNTs catalysts, different TPR profiles have been observed depending on the surface chemistry, particle size and/or location of the metal particles [40]. Therefore, the first reduction peak observed at 380 °C can be assigned to the reduction of NiO nanoparticles located in the exterior wall of the CNT [32]. The reduction peak observed at a lower temperature centered at 291 °C can be assigned to the reduction of NiO nanoparticles with different strengths of interaction with the support or to the reduction of NiO dispersed inside of the CNTs [41]. A similar behavior has been reported for Ru/CNTox catalysts [33]. These results suggest that the metal nanoparticles located inside of the tubes can be reduced more easily than those on the external surface [42] due to the reduced activity of the CNT inner surface compared to the defective outer surface. Considering that the previous oxidation step may have opened the ends of the CNTs to some extent, this may explain the presence of the peak observed at lower reduction temperature, which is in good agreement with results reported by Ding *et al.* [43].

Furthermore, while a decrease reduction signal at 380 °C can be seen, an increase reduction signal at 291 °C over the $Ni/CNTox_1$ and $Ni/CNTox_2$ catalysts can be detected. This behavior is associated to preferential deposition of Ni nanoparticles inside of the nanotubes due to capillary forces of the tubes [43]. Additionally, it has been reported that the H_2 consumption peak observed at higher temperatures around 487 °C is associated with the reduction of supports CNTs since supported transition metals can act as catalysts for the formation of methane via a reaction of hydrogen with the CNTs at higher temperatures [44].

HR-TEM micrographs of the Ni/CNTs catalysts with their respective histograms of their size distribution of the Ni nanoparticle are depicted in Fig. 6. As can be seen in Fig. 6**a-b**, the pristine CNTp consists of long straight graphitic walls with barely any defects or amorphous carbon on the surface. Furthermore, most of the ends of the pristine CNTs are closed and display an inner diameter of about 5 nm (see Fig. 6b). Moreover, it can be clearly observed that the majority of Ni nanoparticles are deposited in the exterior wall of CNT (see Fig. S1), which agrees with the single Ni reduction peak observed at higher temperatures by H_2-TPR. Based upon Fig. 6c-f, it can be observed that both oxidized CNTs have a higher number of defects in their graphitic walls. Some bundles appear exfoliated and curled, suggesting that both acid treatments favor the creation of defects through the formation of surface oxygen groups, which goes hand in hand with the He-TPD/MS results. Furthermore, this process leads to the formation of additional amorphous carbon nanoparticles covering the remaining smaller bundles of CNT (see Fig. 6f) after extended exposure to acid treatments, in agreement with Bower *et al.* [45]. Moreover, the majority of the CNT ends are opened, which enabled the deposition of Ni nanoparticles in the interior of CNTs. These results agree well with the H_2-TPR results. Moreover, the histograms of Ni particle size distribution of the Ni/CNTp, $Ni/CNTox_1$ and $Ni/CNTox_2$ catalysts show a distribution centered at 6.3 ± 0.3, 3.7 ± 0.2 and 2.8 ± 0.1 nm, respectively. These results imply that Ni particle size decreases with an increasing severity of the oxidative functionalization thus highlighting that surface oxygen groups formation improves the dispersion of Ni nanoparticles.

In order to estimate the metal dispersion of Ni nanoparticles, CO chemisorption was performed. The respective results are summarized in Table 2. When Ni metallic particles were deposited over oxidized $CNTox_1$ and $CNTox_2$, a pronounced increase of the CO uptake has been detected. In Table 2, the dispersion expressed as CO/Ni atomic ratio is given. Compared to the Ni/CNTp catalyst, the CO/Ni atomic ratio increase by 5.7 and 14.8 times for the $Ni/CNTox_1$ catalyst the $Ni/CNTox_2$, respectively. This suggests that there is an improvement of Ni nanoparticles dispersion due to the generation of surface functional groups over the supports after both nitric acid and acid mixture functionalization. This is in agreement with previously published research work [46] and with the presented He-TPD/MS results. Additionally, the Ni crystal particle size decreases with an increase in the severity of the oxidative treatment, which is in concordance with the observed tendencies in HR-TEM. These results confirm that the increase of surface oxygen groups, achieved by acid functionalization, improves the Ni dispersion over the support.

Fig. 7a-c shows the XPS of Ni $2p_{3/2}$ region of the different catalysts with 10 wt% Ni loading. Curve fitting of the spectra revealed three partially overlapping contributions for all catalysts. Table 3 summarizes the binding energies (BE) of the most intense Ni $2p_{3/2}$ component, their relative proportion (shown in parentheses) and the Ni/C and Ni/O atomic surface ratio. All catalysts display a BE at 852.8 ± 0.1 eV

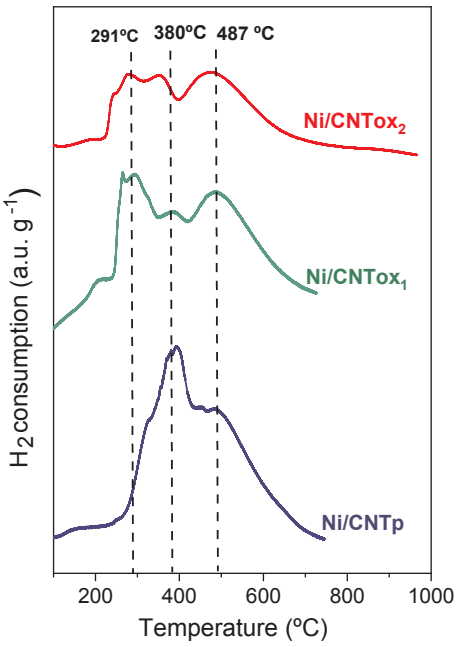

Fig. 5. H_2-TPR profiles of the calcined Ni/CNTs nanohybrid catalysts.

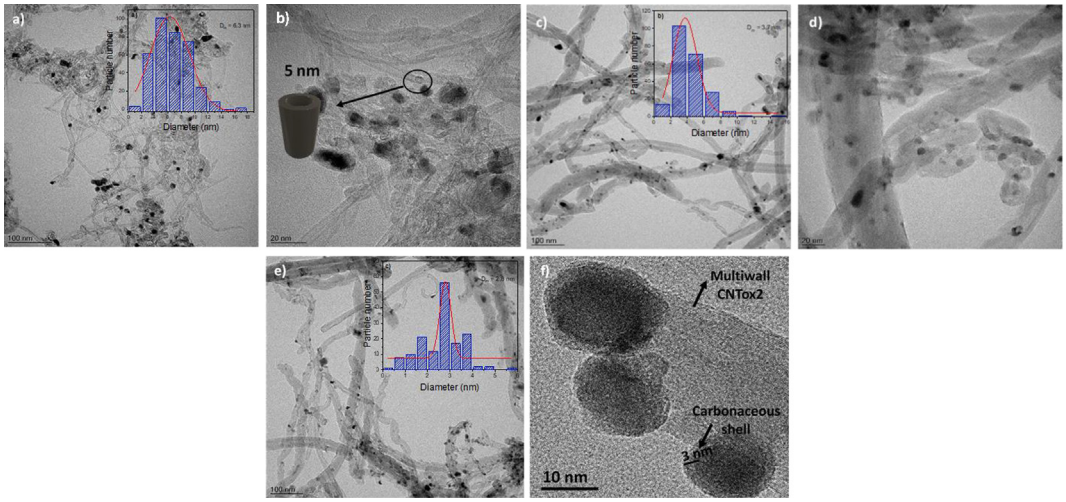

Fig. 6. HR-TEM micrographs of the different reduced catalysts: a) and b) Ni/CNTp, c) and d) Ni/CNTox$_1$ and e) and f) Ni/CNTox$_2$.The insets show the particle size distribution of the nickel nanoparticles.

Table 2
Metal dispersion of the Ni/CNTs catalysts obtained by CO chemisorption.

Catalysts	CO uptake	CO/Ni	Crystal size
	($cm^3\ g^{-1}$)		(nm)
Ni/CNTp	3.73	0.098	7
Ni/CNTox$_1$	21.5	0.563	2
Ni/CNTox$_2$	55.13	1.44	0.7

Table 3
Binding energies (eV) of core levels and atomic ratios of the catalysts.

Catalysts	C1s (eV)	O1s (eV)	Ni $2p_{3/2}$ (eV)	Ni/C (atom/atom)	O/C (atom/atom)
Ni/CNTp	284.8 (80) 286.2 (15) 287.8 (5)	530.4 (19) 531.4 (28) 532.6 (34) 533.8 (19)	852.8 (88) 855.9 (12)	0.005	0.036
Ni/CNTox$_1$	284.8 (82) 286.1 (14) 287.9 (4)	530.4 (17) 531.4 (18) 532.6 (34) 533.8 (31)	852.9 (87) 856.0 (13)	0.007	0.035
Ni/CNTox$_2$	284.8 (83) 286.2 (13) 288.0 (4)	530.4 (12) 531.4 (23) 532.6 (27) 533.8 (38)	852.9 (89) 856.1 (11)	0.008	0.053

assigned to Ni^0 and a BE at 855.9 ± 0.1 eV corresponding to NiO species [41]. Additionally, all catalysts show a satellite peak with a BE of 860.0 ± 0.1 eV, thus confirming the presence of Ni^{2+} [46]. Fig. 7 also shows that the relative proportion (shown in parenthesis) of Ni^0 is much higher than the Ni^{2+} for all catalysts, suggesting that some Ni species strongly interact with the support. Furthermore, Table 3 also summarizes the BEs of the C1s and O1s regions of the catalysts (spectra not shown). It can be observed for all catalysts that the C1s peak had three contributions located at 284.8, 286.2 and 287.8 ± 0.1 eV, while the O1s peak had four contributions located at BEs of 530.4, 531.4, 532.6 and 533.8 ± 0.1 eV. In this regard, the contribution of the C1s with a BE at 284.8 eV represents graphitic carbon [32,34]; while the C1s contribution located at 286.2 eV and the O1s signal at 532.6 eV correspond to the C–O bonds in the phenolic and/or ether groups [46]. Carboxyl/carbonyl groups can be correlated with the contribution located at 287.7 eV (C1s signal) as well as 530.4 and 531.4 eV (O1s signal) [47]. The contribution at 533.8 eV of the O1s signal can be

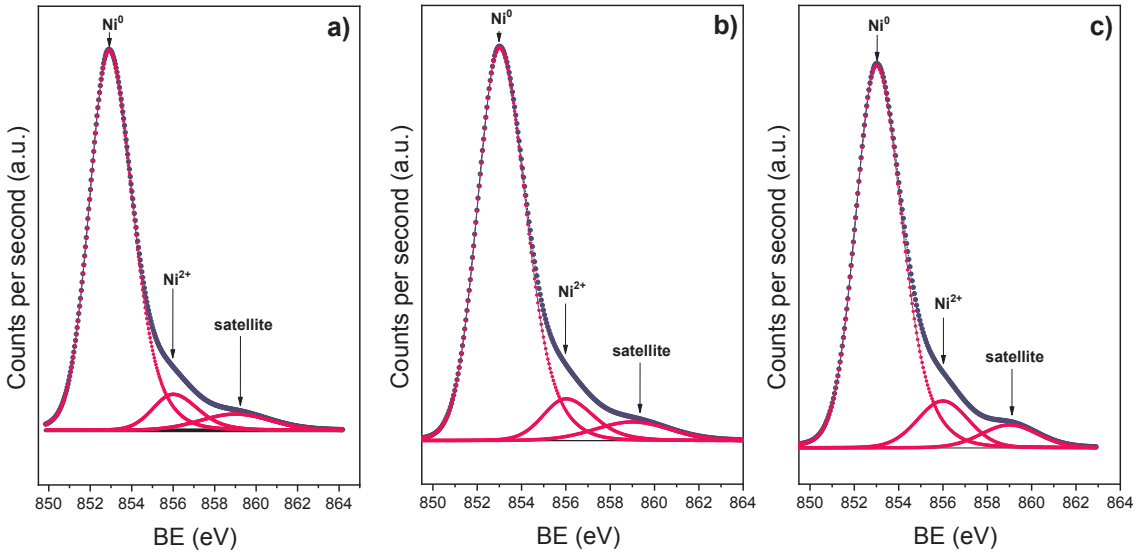

Fig. 7. XPS spectra of the Ni_{2p} region for the reduced a) Ni/CNTp, b) Ni/CNTox$_1$ and c) Ni/CNTox$_2$ catalysts.

assigned to the C-O bonds in carboxylic anhydride groups.

Additionally, the relative ratios (C1s region, shown in parentheses) indicate the predominant existence of graphitic carbon on the surface of all samples. Moreover, it can be deduced that the relative ratios (O1s region) associated with carboxylic acid, carbonyl groups and phenolics/ethers species decrease compared to the untreated catalyst. However, it must be mentioned that the relative proportion of oxygen species associated to anhydride carboxylic groups (BE at 533.8 ± 0.1 eV) of the $Ni/CNTox_1$ and $Ni/CNTox_2$ catalysts increased compared to the Ni/CNTp catalyst. These results suggest that the oxidative treatment favors the anhydride carboxylic formation in CNTs, which is in good agreement with He-TPD/MS results. The Ni/C and O/C atomic surface ratios of the catalysts are also presented in Table 3. In case of $Ni/CNTox_1$ and $Ni/CNTox_2$ catalysts, a slight increase of the Ni/C atomic surface ratio can be observed. According to the CO chemisorption results, a remarkable increase in the dispersion was obtained (the dispersion increases by a factor of 5.7 and 14.8 for $Ni/CNTox_1$ and $Ni/CNTox_2$, respectively). As mentioned before, a loss in the graphitic structure can be seen after acid treatments thus increasing the number of carbon atoms. At the same time, the number of Ni nanoparticles increased over the surface, which leads to the conclusion that the increase of the Ni/C atomic surface ratio is not significant. The same behavior has been observed over the O/C atomic surface ratio over the $Ni/CNTox_1$ catalyst, for which the increase was not significant compared to Ni/CNTp catalyst. However, it can be seen that the O/C atomic surface ratio over the $Ni/CNTox_2$ catalyst increases despite of the loss of the graphitic structure, which implies a significantly increased of the number of oxygen atoms. These results agree well with N_2 physisorption and He-TPD/MS results, and confirm the improvement of Ni nanoparticles dispersion due to the increased amount of oxygen containing surface groups.

To evaluate the wettability of the Ni/CNTs catalysts, the static contact angle was measured on the catalysts' surfaces. Some images are exemplarily depicted in Fig. 8. It has been reported that hydrophilic nanoparticles with a contact angle below 90° tend to form oil-in-water emulsion (o/w), while hydrophobic nanoparticles with a contact angle above 90° are likely to form water-in-oil emulsion droplets (w/o) [29]. As can be seen in Fig. 8, the Ni/CNTp catalyst shows a contact angle of 143°, which is characteristic for materials with a strong hydrophobic character. The nitric acid-functionalized catalyst ($Ni/CNTox_1$) shows a reduced contact angle of about 127°. In contrast, after acid mixture treatment, the $Ni/CNTox_2$ catalyst only displayed a contact angle of 25°. These results indicate that the oxidative treatment using HNO_3 reduced the hydrophobic character of the CNTs in a controlled way thus making them more amphiphilic. An increased in the severity of the functionalization treatment (HNO_3 and H_2SO_4 mixture) drastically decreases the contact angle thus ending up in a considerably hydrophilic material. These results combined with He-TPD/MS and XPS results point to the fact that the increase of surface oxygen groups produces a reduction of the hydrophobic character to obtain an amphiphilic solid. Nevertheless, a further increase of the amount of surface oxygen groups leads to a rather hydrophilic wetting behavior.

In Pickering emulsions, fine amphiphilic solid particles adsorbed at the water/oil interface sterically hinder the coalescence of droplets and effectively stabilize the emulsion [21]. In order to investigate the emulsifier properties of the different Ni/CNTs catalysts, optical/fluorescent micrographs were obtained. Their results are shown in Fig. 9 and Fig. S2a.

All emulsions were prepared under similar experimental conditions while keeping the water/oil ratio and the mass of catalysts constant. When the mixture of water-dodecane was sonicated in presence of the $Ni/CNTox_1$ catalyst, the amphiphilic particles were dispersed at the liquid–liquid interface and an effective formation of emulsion droplet was observed (Fig. 9a). Moreover, it can be seen that the emulsion displays a homogeneous droplets size with an average size of 34.5 μm. After having added a fluorescent and water-soluble dye, it was possible to identify the type of emulsion formed over $Ni/CNTox_1$ catalyst. In Fig. 9b, it can be observed that the internal area of the emulsion droplets presented fluorescence thus proving that the amphiphilic $Ni/CNTox_1$ particles are capable to effectively form w/o emulsion droplets. It has been reported that completely hydrophilic (or hydrophobic) particles may show the tendency to be solely in one of the phases thus reducing the stability of the emulsions [48]. In Fig. S2a, the optical micrographs of emulsion droplets formed by the other Ni/CNTs

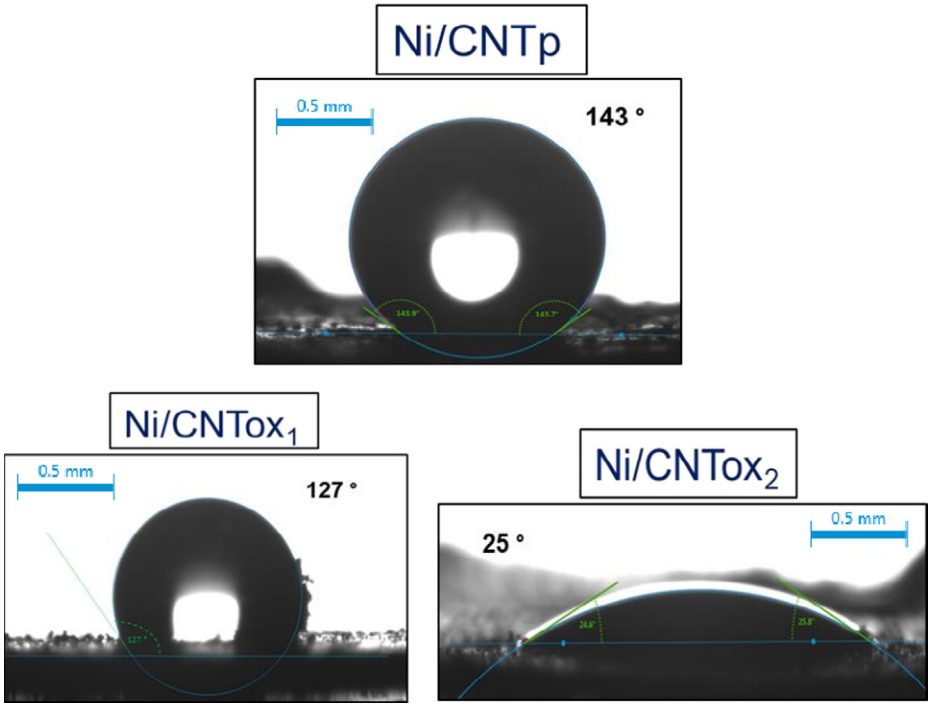

Fig. 8. Static contact angle for the Ni/CNTs catalysts. The photos were immediately captured after having reached equilibrium conditions on the surface of the self-supporting pressed discs.

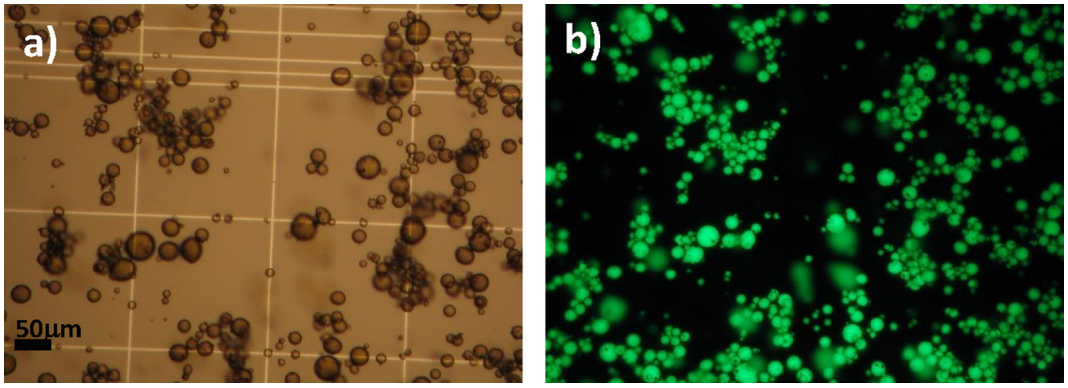

Fig. 9. a) Optical and b) fluorescent microscope images of w/o emulsion droplets stabilized over Ni/CNTox$_1$ catalysts. Water-soluble dye and fluorescent (green color, fluorescent Na salt) were added to identify the emulsion's type. (For interpretation of the references to color in this figure legend, the reader is referred to the web version of this article.)

catalysts are summarized.

It can be clearly observed that after sonication of water-dodecane mixture with both Ni/CNTp and Ni/CNTox$_2$ catalysts no emulsion droplets were observed. This result suggests that if the particles are very hydrophobic (Ni/CNTp, high θ = 143°) or very hydrophilic (Ni/CNTox$_2$, low θ = 25°), they tend to remain dispersed in either the organic or the aqueous phase (Fig. S2b). This result in unstable droplets that quickly coalescence after their formation. This, in turn, implies that, if the surface of solid particles presents either a low or high concentration of oxygen groups (Ni/CNTp or Ni/CNTox$_2$, respectively), stable emulsions cannot be formed. Therefore, the tailored wettability of the catalyst adjusted by the severity of acid treatments plays a key role with respect to the formation of stable emulsions.

3.2. Hydrogenation of furfural

Since the biomass-derived bio-oil is a complex liquid that is partially soluble either in water or hydrocarbon solvents, the hydrogenation reaction in water–oil systems are more desirable from a practical view. Therefore, catalytic conversion of furfural, as a preliminary reaction, in water–dodecane Pickering emulsions stabilized by Ni/CNTs catalysts was investigated. The corresponding results are shown in Fig. 10. It is observed that when the reaction takes place over the Ni/CNTp catalyst, the conversion of FAL reaches 63% after a reaction of 4 h.

Under identical reaction conditions, the oxidized Ni/CNTox$_1$ catalyst showed the highest conversion of FAL (94%), while the Ni/CNTox$_2$ catalyst only reached a decreased FAL conversion of 55%. The increase in FAL conversion up to 94% for the Ni/CNTox$_1$ catalyst can be attributed to an improvement of the Ni metal dispersion due to an increased amount of surface oxygen groups, which agrees well with results obtained by CO chemisorption, HR-TEM, XPS and He/TPD-MS. Nevertheless, the decrease of FAL conversion over Ni/CNTox$_2$ cannot be correlated with metal dispersion. This implies that there are other parameters affecting the catalytic activity, such as the wettability of the solid nanoparticles. The lowest and highest amount of surface oxygen groups over the Ni/CNTp and Ni/CNTox$_2$ catalysts induce a rather hydrophilic and hydrophobic character, respectively, thus avoiding the formation of stable emulsion droplets as confirmed by the static contact angle measurements and optical micrographs analysis (Fig. S2a). Therefore, the lower FAL conversion observed over Ni/CNTp and Ni/CNTox$_2$ can be related to the lack of the formation of stable emulsion droplets. Catalytic reactions performed in biphasic media tend to be slower compared to the conversion in emulsion droplets as reported by Jimaré *et al.* [49]. They reported that the formation of stable emulsions remarkably increases the value of the volumetric global mass transport coefficients due to the increased interfacial area. By increasing the mass transport coefficients by solid-particle stabilized emulsification, the reaction rate can be greatly enhanced. Therefore, the catalytic activity results and the amphiphilic properties of the Ni-based catalysts suggest that the conversion of FAL over Ni/CNTp and Ni/CNTox$_2$ catalysts was carried out in a biphasic medium rather than an emulsion system. This procures several issues related to the diffusion of reactants to active sites, thus lowering the resulting catalytic activity. In conclusion, all results indicate that the highest FAL conversion reached over Ni/CNTox$_1$ catalyst is achieved by two phenomena: an overall improvement of the Ni metal dispersion together with the possibility to form stable emulsion droplets, which was achieved by a controlled increase of surface oxygen groups during the HNO_3 functionalization. Fig. 10 shows the yield of the reaction products obtained during FAL conversion over the different Ni-based CNT catalysts after a reaction time of 4 h. It can be seen that the main product over Ni/CNTp is cyclopentanone (CPO, 54%), followed by levulinic acid (LA, 5.3%) and furfuryl alcohol (FUR-OH,1.5%) as secondary products. When FAL was converted over Ni/CNTox$_1$, an increase of CPO selectivity (69%) was observed. As secondary products, cyclopentanol (CPOL, 10%), tetrahydrofurfuryl alcohol (THF-OH, 7%) and LA (6%) have been detected. For the reaction over Ni/CNTox$_2$, two mains products can be verified: LA (22%) and CPO (28%). Traces of furfuryl alcohol (FUR-OH, 1%) have been measured.

It has already been reported in the literature that furfural can be converted to fuel additive as well as value-added chemicals through different reactions [50]. Fig. 11 shows the main products obtained in

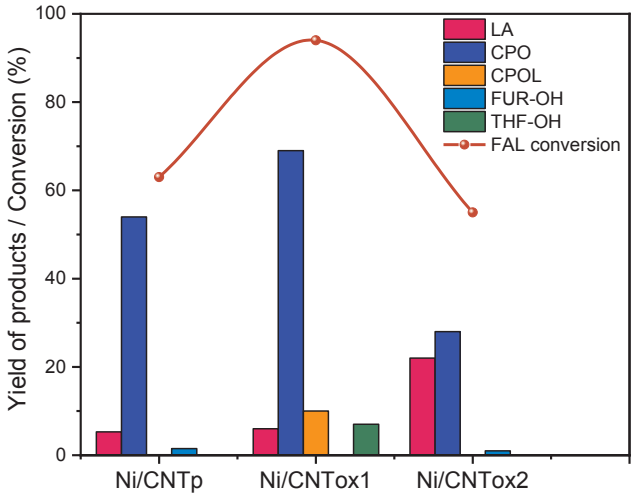

Fig. 10. Catalytic activity and yield of products in the hydrogenation of furfural over Ni/CNT-functionalized catalysts. Reaction conditions: temperature 200 °C, 2.0 MPa of H_2 and reaction time of 4 h.

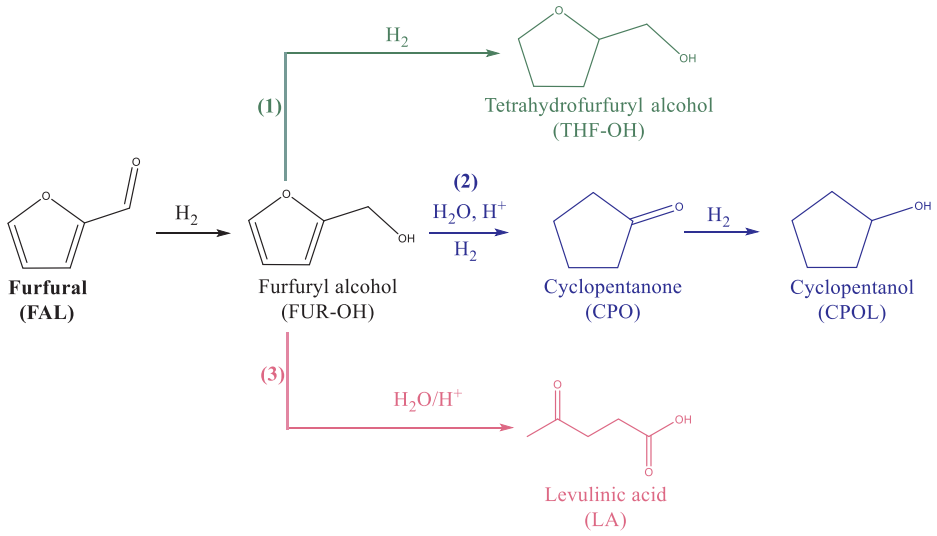

Fig. 11. Main products during the hydrogenation of furfural in water under hydrogen atmosphere and metal–acid catalysts [1,4], showing direct hydrogenation and hydration reactions.

aqueous hydrogenation of furfural in the presence of hydrogen and metal/acid-functional catalysts [51,52].

It can be seen that FAL can be converted to FUR-OH by direct C = O hydrogenation over metallic sites [53]. Then, FUR-OH can be transformed by three principal routes: (1) hydrogenation of C = C ring bond to obtain THF-OH; (2) under reduction conditions and aqueous medium, Piancantelli ring rearrangement [52] can occur to form cyclopentanone, which can be hydrogenated to cyclopentanol and (3) direct ring opening through hydrolysis in acid medium to obtain LA. Bradley *et al.* [54] have shown that the relatively strong adsorption of furfural observed on metals (groups 8–10) is due to the interaction of the π orbitals with the metal d orbitals. This interaction weakens the C-O bond, helping to stabilize a di-sigma complex η^2-(C-O) aldehyde [55]. This behavior may explain the ring opening and rearrangement of furfural to cyclopentanone over Ni/CNTp, Ni/CNTox$_1$ and Ni/CNTox$_2$ catalysts. Furthermore, it has been reported by Hronec *et al.* that when the reaction of furfural was performed under N_2 or H_2 atmosphere without catalysts, no CPO or other products were detected, which indicated that the rearrangement of the furan ring does not occur directly from furfural [56]. Furthermore, during the catalytic conversion of FAL in aqueous phases different reaction intermediates can be formed. For example, 4-hydroxy-2-cyclopentenone (HCP) and its hydrogenation product, 2-cyclopentenone, are two important intermediates in the formation of CPO [16].

However, during the catalytic conversion of FAL over all Ni/CNTs nanohybrid catalysts, these intermediates have not been observed. In a control reaction of HCP over NiCu/SBA-15 catalyst, Yang *et al.* stated that when a limited amount of H_2 was charged, 38% of 2-cyclopentenone was obtained after 4 h, besides a 4% yield of CPO. Nevertheless, after excess of H_2 was introduced into the reactor, 2-cyclopentanone disappeared, while the total yield of CPO and CPOL significantly increased to 39% [15]. Therefore, under H_2 excess (2.0 MPa of H_2), the formation of these intermediate occurs faster, and only CPO can be observed. Additionally, it has been reported that furfuryl alcohol in presence of very strong acids sites rearranged to levulinic acid (4-ketopentanoic acid) [57]. Thus, the increase of medium acid sites observed over Ni/CNTox$_2$ could favor the formation of levulinic acid, which is in concordance with NH_3-TPD analysis.

In order to emphasize the advantages of performing a catalytic reaction in an emulsion system, the FAL conversion was performed in both single aqueous and organic media over the amphiphilic Ni/CNTox$_1$ catalyst. The respective results are displayed in the Fig. 12.

It can be observed that a low FAL conversion was obtained in both phases (3% and 18% in aqueous and organic phase, respectively). The highest FAL conversion in the emulsion phase was observed (34%) after 1 h of reaction. According to these results, the lack of the possibility to form stable emulsion droplets makes the reactant's diffusion to active sites more difficult thus producing a decrease in FAL conversion. Also, a catalyst deactivation produced by the irreversible water adsorption on active sites can not be ruled out [58]. In contrast, the highest FAL conversion obtained in an emulsion system could be attributed to an increase of the interfacial area through the creation of stable emulsion droplets, which enables the diffusion of reactant to active sites. Fig. 12 also shows the yield of the reaction products obtained during FAL conversion in different reaction media over the Ni/CNTox$_1$ catalyst after 1 h of reaction. It is observed that when the reaction was carried out in the organic phase, the main products were furfuryl alcohol (FUR-OH) and 2-methylfuran (2-MF), while tetrahydrofurfuryl alcohol (THF-OH) was obtained in the fewest amount. This suggests that, in the absence of water, only FAL hydrogenation products are obtained. When the reaction is carried out in aqueous medium, the main product observed was cyclopentanone (CPO), while only traces of FUR-OH were obtained. This implies that the presence of water inhibits the hydrogenating capacity of the catalyst to a certain extent. In contrast, when the catalytic conversion of FAL was carried out in an emulsion system, the yield of CPO and LA is increased by a factor of two compared to the

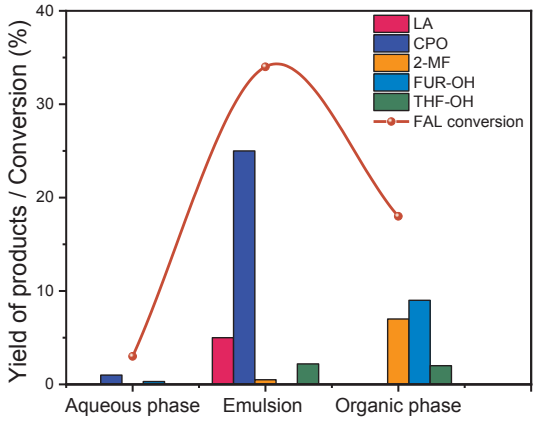

Fig. 12. Catalytic conversion of furfural and yield of products in aqueous, organic and emulsion phases over Ni/CNTox$_1$ amphiphilic catalyst. Reaction conditions: 200 °C, 2.0 MPa of H_2, 0.232 mol L^{-1} of FAL, reaction time of 1 h.

obtained yield in the single phases. In addition, the hydrogenation products of FAL decreased considerably. The results from this study displayed a better catalytic performance (greater activity and high selectivity to cyclopentanone) in comparison to others catalytic systems reported in the literature (Table S1) for liquid phase conversion of furfural, which is a clear indication of the potential of this catalytic system.

One of the main focus of the catalytic emulsion systems is to isolate target products from the reaction medium due to differences in the relative solubilities. However, not all the solubility values of a given compound are available. Therefore, a parameter that can help to predict the solubility behavior of a given molecule in a water/oil system is the octanol–water partition coefficient (log P). This value has been widely used as a measure of the hydrophobicity/hydrophilicity ratio of a molecule. High log P values indicate a higher affinity of the molecule to the organic phase, and vice versa. Fig. 13 shows the partition of the reaction products between both organic and aqueous phases over different Ni/CNTs catalysts. It can be seen that when FAL conversion was carried out over Ni/CNTp, the reaction products CPO and LA were mostly solubilized in the aqueous phase. When FAL is converted over Ni/CNTox$_2$, CPO is partitioned in equal amounts between the aqueous and organic phase, while LA was mostly solubilized in the organic phase. Adsorption of solid particles at the water–oil interface requires the partial wetting of the solid by both water and oil. In fact, highly hydrophilic solid particles could be totally wetted by water, whereas highly hydrophobic solid particles could be totally wetted by oil. This characteristic hinders that the solid particles can be adsorbed at the interface, thus avoiding the formation of stable emulsion droplets since they remain dispersed either in the aqueous or the oil phase of the biphasic system [59]. Because of that, Ni/CNTp (hydrophobic particles) and Ni/CNTox$_2$ (hydrophilic particles) may convert mainly FAL in a biphasic system rather than in an emulsion system, in concordance to contact angle measurement and optical micrograph analysis. Furthermore, the lack of stable emulsion droplets disfavors the diffusion of the formed products towards the phase of higher solubility. In fact, the log P value of LA is about −0.35 thus indicating that this species should be solubilized in the aqueous phase. However, over the Ni/CNTox$_2$ catalyst, the opposite behavior observed, which confirms the mentioned diffusion problem of the formed products in a biphasic system. Moreover, the Ni/CNTox$_1$ catalyst shows that LA was mostly soluble in the aqueous phase and the

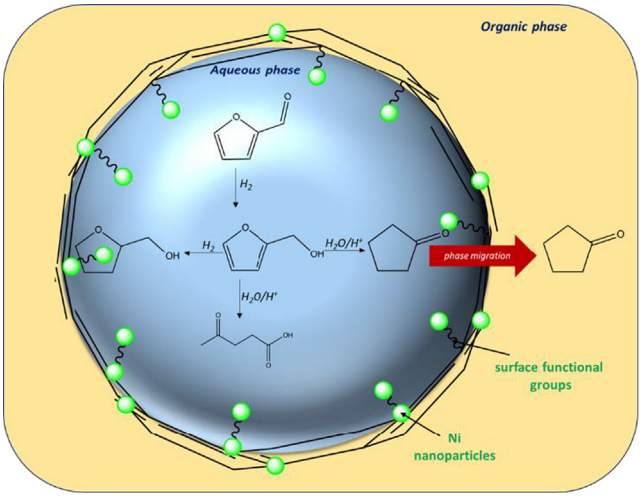

Fig. 14. Schematic illustration of catalytic reaction taking place at the water–oil interface in the solid-stabilized emulsion droplet over the Ni/CNTox$_1$ catalyst.

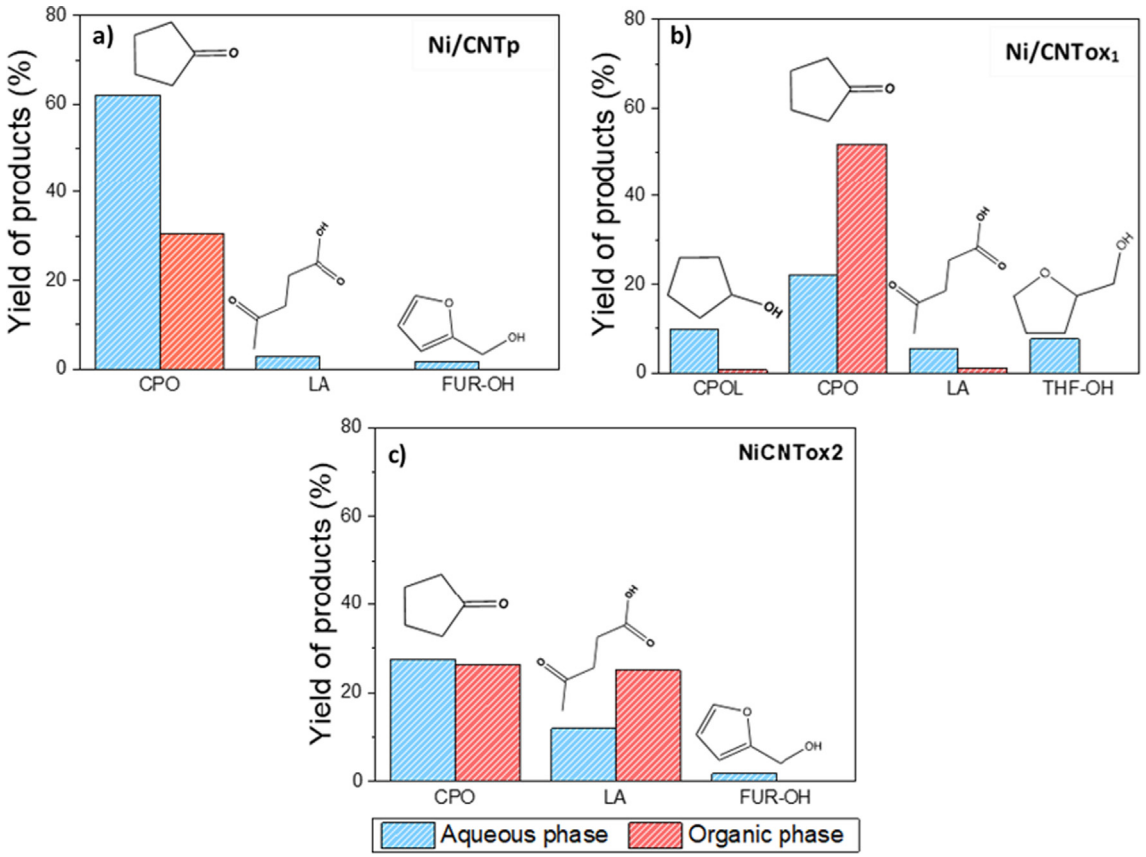

Fig. 13. Partition of the products in the organic and aqueous phase after 4 h of reaction over a) Ni/CNTp b) Ni/CNTox$_1$ and c) Ni/CNTox$_2$ catalysts. Reaction conditions: FAL (0.232 mol L^{-1}), Ni/CNTs (Ni: 10 wt%), solvents (dodecane 25 mL, water 25 mL), 200 °C and 2.0 MPa of H_2.

target product CPO was highly soluble in the organic phase, in agreement with log P values (log P CPO, 0.89; log P LA, −0.35). This result implies that Ni/CNTox$_1$ catalyst allowed for the formation of stable emulsion droplets, which enables the migration of CPO to the organic phase after its formation. In contrast, LA remains in the aqueous phase. This behavior is shown in Fig. 14, in which a water–oil emulsion droplet is schematically depicted. These results for the Ni/CNTox$_1$ catalyst illustrate the simultaneous reaction and separation of reaction products in Pickering emulsions, thus drastically simplifying the isolation stages and the purification of the target products.

4. Conclusions

Amphiphilic CNT-supported Ni particles have been prepared and their emulsifying properties for the hydrogenation of furfural (biomass-derived furanic compounds) have been tested at the water–oil interface. Prior to their usage, the wettability of the catalysts was tuned by adjusting the severity of acid treatments during the catalysts' synthesis. In order to do so, pristine CNTs were modified either by nitric acid (CNTox$_1$) or impregnated with a mixture of nitric and sulfuric acid (CNTox$_2$). It was found that the wettability of the catalyst played an essential role in forming stable emulsions and the enhancement of catalytic activity. The catalytic activity increased when the conversion of FAL was carried out over Ni/CNTox$_1$, which can be traced back to an improved Ni metal dispersion together with the possible formation of stable emulsion droplets due to a gradual increase of the amount of surface oxygen groups and its amphiphilic character. In contrast, the lower FAL conversion observed over both Ni/CNTp (highly hydrophobic particles) and Ni/CNTox$_2$ (highly hydrophilic particles) catalysts, although having a good dispersion of Ni nanoparticles achieved over Ni/CNTox$_2$ catalyst, was attributed to the missing possibility form stable emulsion droplets. In terms of the yield of reaction products, Ni/CNTp and Ni/CNTox$_2$ catalysts displayed a yield to CPO formation with high solubility in the aqueous phase. In contrast, the Ni/CNTox$_1$ catalyst demonstrated the highest selectivity regarding the formation of CPO with high solubility in the organic phase. The results obtained over the amphiphilic Ni/CNTox$_1$ catalyst highlight the simultaneous reaction and separation of the target product in Pickering emulsion, thus simplifying the isolation stages of the key products. This offers an excellent strategy to overcome the conventional phase-transfer catalysis limitation for biomass and its-derived compounds (such as furfural) conversion.

Credit authorship contribution statement

C. Herrera: Conceptualization, Methodology, Investigation, Writing - original draft. **L. Barrientos:** . **A. Rosenkranz:** . **C. Sepulveda:** . **J.L. García-Fierro:** . **M.A. Laguna-Bercero:** . **N. Escalona:** Resources, Investigation, Supervision.

Declaration of Competing Interest

The authors declare that they have no known competing financial interests or personal relationships that could have appeared to influence the work reported in this paper.

Acknowledgments

The authors are grateful to CONICYT-Chile for FONDECYT N° 1180982, FONDEQUIP EQM 160070, PIA CCTE AFB 170007 project and CONICYT doctoral scholarship N° 21170881. The authors also gratefully thank the Chilean Ministry of Economy, Development and Tourism within the framework of the Millennium Science Initiative program for the grant "Nuclei on Catalytic Processes towards Sustainable Chemistry (CSC)". A. Rosenkranz gratefully acknowledges the financial support given by CONICYT-Chile for FONDECYT N° 11180121 and the VID of the University of Chile in the framework of U-Inicia UI 013/2018. The use of Servicio General de Apoyo a las Investigación (SAI, University of Zaragoza) is also acknowledged. The authors also gratefully the support for the research performed to J. L. García-Fierro (R.I.P.).

Appendix A. Supplementary data

Supplementary data to this article can be found online at https://doi.org/10.1016/j.fuel.2020.118032.

References

[1] Climent MJ, Corma A, Iborra S. Conversion of biomass platform molecules into fuel additives and liquid hydrocarbon fuels. Green Chem. 2014;16:516–47. https://doi.org/10.1039/C3GC41492B.
[2] Rodhe H. A comparison of the contribution of various gases to the greenhouse effect. Science 1990;248:1217–9. https://doi.org/10.1126/science.248.4960.1217.
[3] Mullen CA, Boateng AA. Chemical composition of bio-oils produced by fast pyrolysis of two energy crops. Energy Fuels 2008;22:2104–9. https://doi.org/10.1021/ef700776w.
[4] Nakagawa Y, Tamura M, Tomishige K. Catalytic Reduction of Biomass-Derived Furanic Compounds with Hydrogen. ACS Catal. 2013;3:2655–68. https://doi.org/10.1021/cs400616p.
[5] Resasco DE, Crossley SP. Implementation of concepts derived from model compound studies in the separation and conversion of bio-oil to fuel. Catal. Today. 2015;257:185–99. https://doi.org/10.1016/j.cattod.2014.06.037.
[6] Runnebaum RC, Nimmanwudipong T, Block DE, Gates BC. Catalytic conversion of compounds representative of lignin-derived bio-oils: a reaction network for guaiacol, anisole, 4-methylanisole, and cyclohexanone conversion catalysed by Pt/γ-Al2O3. Catal. Sci. Technol. 2012;2:113–8. https://doi.org/10.1039/C1CY00169H.
[7] Zhang X, Zhang Q, Wang T, Ma L, Yu Y, Chen L. Hydrodeoxygenation of lignin-derived phenolic compounds to hydrocarbons over Ni/SiO2-ZrO2 catalysts. Bioresour. Technol. 2013;134:73–80. https://doi.org/10.1016/j.biortech.2013.02.039.
[8] Bohre A, Dutta S, Saha B, Abu-Omar MM. Upgrading Furfurals to Drop-in Biofuels: An Overview. ACS Sustain. Chem. Eng. 2015;3:1263–77.
[9] Yan K, Jarvis C, Gu J, Yan Y. Production and catalytic transformation of levulinic acid: A platform for speciality chemicals and fuels. Renew. Sustain. Energy Rev. 2015;51:986–97. https://doi.org/10.1016/j.rser.2015.07.021.
[10] Zhou M, Li J, Wang K, Xia H, Xu J, Jiang J. Selective conversion of furfural to cyclopentanone over CNT-supported Cu based catalysts: Model reaction for upgrading of bio-oil. Fuel 2017;202:1–11. https://doi.org/10.1016/j.fuel.2017.03.046.
[11] Ordomsky VV, J.c. Schouten, J. Van Der Schaaf, T.A. Nijhuis. Biphasic single-reactor process for dehydration of xylose and hydrogenation of produced furfural. Appl. Catal. A Gen. 2013;451:6–13. https://doi.org/10.1016/j.apcata.2012.11.013.
[12] Date NS, Kondawar SE, Chikate RC, Rode CV. Single-Pot Reductive Rearrangement of Furfural to Cyclopentanone over Silica-Supported Pd Catalysts. ACS Omega 2018;3:9860–71.
[13] Hronec M, Fulajtarová K. Selective transformation of furfural to cyclopentanone. Catal. Commun. 2012;24:100–4. https://doi.org/10.1016/j.catcom.2012.03.020.
[14] Y. Liu, Z. Chen, X. Wang, Y. Liang, X. Yang, Z. Wang, Highly Selective and Efficient Rearrangement of Biomass-Derived Furfural to Cyclopentanone over Interface-Active Ru/Carbon Nanotubes Catalyst in Water, ACS Sustain. Chem. Eng. 5 (2017) 744–751. http://doi.org/10.0.3.253/acssuschemeng.6b02080.
[15] Yang Y, Du Z, Huang Y, Lu F, Wang F, Gao J, et al. Conversion of furfural into cyclopentanone over Ni-Cu bimetallic catalysts. Green Chem. 2013;15:1932–40. https://doi.org/10.1039/c3gc37133f.
[16] Hronec M, Fulajtárová K, Vávra I, Soták T, Dobročka E, Mičušík M. Carbon supported Pd-Cu catalysts for highly selective rearrangement of furfural to cyclopentanone. Appl. Catal. B Environ. 2016;181:210–9. https://doi.org/10.1016/j.apcatb.2015.07.046.
[17] Li XL, Deng J, Shi J, Pan T, Yu CG, Xu HJ, et al. Selective conversion of furfural to cyclopentanone or cyclopentanol using different preparation methods of Cu-Co catalysts. Green Chem. 2015;17:1038–46. https://doi.org/10.3390/catal8050193.
[18] Bhanja P, Bhaumik A. Porous nanomaterials as green catalyst for the conversion of biomass to bioenergy. Fuel 2016;185:432–41. https://doi.org/10.1016/j.fuel.2016.08.004.
[19] Hutchings GS, Luc W, Lu Q, Zhou Y, Vlachos DG, Jiao F. Nanoporous Cu–Al–Co Alloys for Selective Furfural Hydrodeoxygenation to 2-Methylfuran. Ind. Eng. Chem. Res. 2017;56:3866–72. https://doi.org/10.1021/acs.iecr.7b00316.
[20] Chiaramonti D, Bonini M, Fratini E, Tondi G, Gartner K, Bridgwater AV, et al. Development of emulsions from biomass pyrolysis liquid and diesel and their use in engines - Part 1: Emulsion production. Biomass Bioenergy 2003;25:85–99. https://doi.org/10.1016/S0961-9534(02)00183-6.
[21] Pera-Titus M, Leclercq L, Clacens JM, De Campo F, Nardello-Rataj V. Pickering interfacial catalysis for biphasic systems: From emulsion design to green reactions. Angew. Chemie - Int. Ed. 2015;54:2006–21. https://doi.org/10.1002/anie.

201402069.
[22] He Y, Wu F, Sun X, Li R, Guo Y, Li C, et al. Factors that affect Pickering emulsions stabilized by graphene oxide. ACS Appl Mater Interfaces. 2013;5:4843–55. https://doi.org/10.1021/am400582n.
[23] Tang M, Wang X, Wu F, Liu Y, Zhang S, Pang X, et al. Au nanoparticle/graphene oxide hybrids as stabilizers for Pickering emulsions and Au nanoparticle/graphene oxide@polystyrene microspheres. Carbon N. Y. 2014;71:238–48. https://doi.org/10.1016/j.carbon.2014.01.034.
[24] Zapata PA, Faria J, Ruiz MP, Jentoft RE, Resasco DE. Hydrophobic Zeolites for Biofuel Upgrading Reactions at the Liquid − Liquid Interface in Water / Oil Emulsions. J. Am. Chem. Soc. 2012;134:8570–8. https://doi.org/10.1021/ja3015082.
[25] Crossley S, Faria J, Shen M, Resasco DE. Solid nanoparticles that catalyze biofuel upgrade reactions at the water/oil interface. Science 2010;327:68–72. https://doi.org/10.1126/science.1180769.
[26] Zhu Z, Tan H, Wang J, Yu S, Zhou K. Hydrodeoxygenation of vanillin as a bio-oil model over carbonaceous microspheres-supported Pd catalysts in the aqueous phase and Pickering emulsions. Green Chem. 2014;16:2636–43. https://doi.org/10.1039/C3GC42647E.
[27] Yang X, Liang Y, Cheng Y, Song W, Wang X, Wang Z, et al. Hydrodeoxygenation of vanillin over carbon nanotube-supported Ru catalysts assembled at the interfaces of emulsion droplets. Catal. Commun. 2014;47:28–31. https://doi.org/10.1016/j.catcom.2013.12.027.
[28] Zapata PA, Faria J, Pilar Ruiz M, Resasco DE. Condensation/hydrogenation of biomass-derived oxygenates in water/oil emulsions stabilized by nanohybrid catalysts. Top. Catal. 55 2012:38–52. https://doi.org/10.1007/s11244-012-9768-4.
[29] Resasco DE. Carbon nanohybrids used as catalysts and emulsifiers for reactions in biphasic aqueous/organic systems. Chinese J. Catal. 2014;35:798–806. https://doi.org/10.1016/S1872-2067(14)60119-4.
[30] Xie Y, Sun M, Shen Y, Li H, Lv G, Cai Z, et al. Preparation of rGO-mesoporous silica nanosheets as Pickering interfacial catalysts. RSC Adv. 2016;6:101808–17. https://doi.org/10.1039/C6RA22389C.
[31] Lam E, Luong JHT. Carbon Materials as Catalyst Supports and Catalysts in the Transformation of Biomass to Fuels and Chemicals. ACS Catal. 2014;4:3393–410. https://doi.org/10.1021/cs5008393.
[32] Martin-Martinez M, Machado BF, Serp P, Morales-Torres S, Silva AMT, Figueiredo JL, et al. Carbon nanotubes as catalysts for wet peroxide oxidation: The effect of surface chemistry. Catal. Today. 2019:1–9. https://doi.org/10.1016/j.cattod.2019.03.014.
[33] B.F. Machado, M. Oubenali, M. Rosa Axet, T. Trang Nguyen, M. Tunckol, M. Girleanu, O. Ersen, I.C. Gerber, P. Serp, Understanding the surface chemistry of carbon nanotubes: Toward a rational design of Ru nanocatalysts, J. Catal. 309 (2014) 185–198. http://doi.org/10.1016/j.jcat.2013.09.016.
[34] Figueiredo JL, Pereira MFR, Freitas MMA, Orfao JJM. Modification of the surface chemistry of activated carbons. Carbon N. Y. 1999;37:1379–89. https://doi.org/10.1016/S0008-6223(98)00333-9.
[35] Ghampson IT, Sepulveda C, Garcia R, Fierro JLG, Escalona N. Carbon nanofiber-supported ReOx catalysts for the hydrodeoxygenation of lignin-derived compounds. Catal. Sci. Technol. 2016;6:4356–69. https://doi.org/10.1039/c5cy01992c.
[36] Datsyuk V, Kalyva M, Papagelis K, Parthenios J, Tasis D, Siokou A, et al. Chemical oxidation of multiwalled carbon nanotubes. Carbon N. Y. 2008;46:833–40. https://doi.org/10.1016/j.carbon.2008.02.012.
[37] Ghampson IT, Pecchi G, Fierro JLG, Videla A, Escalona N. Catalytic hydrodeoxygenation of anisole over Re-MoOx/TiO2 and Re-VOx/TiO2 catalysts. Appl. Catal. B Environ. 2017;208:60–74. https://doi.org/10.1016/j.apcatb.2017.02.047.
[38] Thommes M, Kaneko K, Neimark AV, Olivier JP, Rodriguez-Reinoso F, Rouquerol J, et al. Physisorption of gases, with special reference to the evaluation of surface area and pore size distribution (IUPAC Technical Report). Pure Appl. Chem. 2015;87:1051–69. https://doi.org/10.1515/pac-2014-1117.
[39] Dongil AB, Pastor-Pérez L, Sepúlveda-Escribano A, García R, Escalona N. Hydrodeoxygenation of guaiacol: Tuning the selectivity to cyclohexene by introducing Ni nanoparticles inside carbon nanotubes. Fuel 2016;172:65–9. https://doi.org/10.1016/j.fuel.2016.01.002.
[40] Lu S, Zhang C, Liu Y. Carbon nanotube supported Pt- Ni catalysts for preferential oxidation of CO in hydrogen-rich gases. Int. J. Hydrogen Energy. 2011;36:1939–48. https://doi.org/10.1016/j.ijhydene.2010.11.029.
[41] Ma Q, Wang D, Wu M, Zhao T, Yoneyama Y, Tsubaki N. Effect of catalytic site position: Nickel nanocatalyst selectively loaded inside or outside carbon nanotubes for methane dry reforming. Fuel 2013;108:430–8. https://doi.org/10.1016/j.fuel.2012.12.028.
[42] Dongil AB, Pastor-Pérez L, Fierro JLG, Escalona N, Sepúlveda-Escribano A. Synthesis of palladium nanoparticles over graphite oxide and carbon nanotubes by reduction in ethylene glycol and their catalytic performance on the chemoselective hydrogenation of para-chloronitrobenzene. Appl. Catal. A Gen. 2016;513:89–97. https://doi.org/10.1016/j.apcata.2015.11.048.
[43] Ding Y, Bao X, Luo H, Fan Z, Pan X, Chen W. Enhanced ethanol production inside carbon-nanotube reactors containing catalytic particles. Nat. Mater. 2007;6:507–11. https://doi.org/10.1038/nmat1916.
[44] Yang H, Song S, Rao R, Wang X, Yu Q, Zhang A. Chemical Enhanced catalytic activity of benzene hydrogenation over nickel confined in carbon nanotubes. J. Mol. Catal. A Chem. 2010;323:33–9. https://doi.org/10.1016/j.molcata.2010.03.005.
[45] Bower C, Kleinhammes A, Wu Y, Zhou O. Intercalation and partial exfoliation of single-walled carbon nanotubes by nitric acid. Chem. Phys. Lett. 1998;288:481–6. https://doi.org/10.1016/S0009-2614(98)00278-4.
[46] Dongil AB, Ghampson IT, Garcia R, Fierro JLG, Escalona N. Hydrodeoxygenation of Guaiacol over Ni/Carbon catalysts: Effect of the Support and Ni Loading. RSC Adv. 2016;6:2611–23. https://doi.org/10.1039/c5ra22540j.
[47] Gardner SD, Singamsetty CSK, Booth GL, He G-R. Surface characterization of carbon fibers using angle-resolved xps and iss. Carbon N. Y. 1995;33:587–95. https://doi.org/10.1016/0008-6223(94)00144-O.
[48] Meng T, Bai R, Wang W, Yang X, Guo T, Wang Y. Enzyme-Loaded Mesoporous Silica Particles with Tuning Wettability as a Pickering Catalyst for enhancing biocatalysis. Catalysts. 2019;9:78. https://doi.org/10.3390/catal9010078.
[49] Jimare MT, Cazaña F, Ramirez A, Royo C, Romeo E, Faria J, et al. Modelling of experimental vanillin hydrodeoxygenation reactions in water/oil emulsions. Effects of mass transport. Catal. Today. 2013;210:89–97. https://doi.org/10.1016/j.cattod.2012.11.015.
[50] Yan K, Wu G, Lafleur T, Jarvis C. Production, properties and catalytic hydrogenation of furfural to fuel additives and value-added chemicals. Renew. Sustain. Energy Rev. 2014;38:663–76. https://doi.org/10.1016/j.rser.2014.07.003.
[51] Zhou M, Zhu H, Niu L, Xiao G, Xiao R. Catalytic hydroprocessing of furfural to cyclopentanol over Ni/CNTs catalysts: Model reaction for upgrading of bio-oil. Catal. Lett. 2014;144:235–41. https://doi.org/10.1007/s10562-013-1149-5.
[52] Hronec M, Fulajtarová K, Liptaj T. Effect of catalyst and solvent on the furan ring rearrangement to cyclopentanone. Appl. Catal. A Gen. 2012;437–438:104–11. https://doi.org/10.1016/j.apcata.2012.06.018.
[53] Bhogeswararao S, Srinivas D. Catalytic conversion of furfural to industrial chemicals over supported Pt and Pd catalysts. J. Catal. 2015;327:65–77. https://doi.org/10.1016/j.jcat.2015.04.018.
[54] Bradley MK, Robinson J, Woodruff DP. The structure and bonding of furan on Pd (111). SUSC. 2010;604:920–5. https://doi.org/10.1016/j.susc.2010.02.021.
[55] Sitthisa S, Resasco DE. Hydrodeoxygenation of Furfural Over Supported Metal Catalysts : A Comparative Study of Cu, Pd and Ni. Catal. Letters. 2011;141:784–91. https://doi.org/10.1007/s10562-011-0581-7.
[56] Hronec M, Fulajtárová K, Soták T. Kinetics of high temperature conversion of furfuryl alcohol in water. J. Ind. Eng. Chem. 2014;20:650–5. https://doi.org/10.1016/j.jiec.2013.05.029.
[57] Lange JP, van de Graaf WD, Haan RJ. Conversion of furfuryl alcohol into ethyl levulinate using solid acid catalysts. ChemSusChem 2009;2:437–41. https://doi.org/10.1002/cssc.200800216.
[58] Mironenko RM, Belskaya OB, Gulyaeva TI, Nizovskii AI, Kalinkin AV, Bukhtiyarov VI, et al. Effect of the nature of carbon support on the formation of active sites in Pd/C and Ru/C catalysts for hydrogenation of furfural. Catal. Today. 2015;249:145–52. https://doi.org/10.1016/j.cattod.2014.10.037.
[59] Chevalier Y, Bolzinger MA. Emulsions stabilized with solid nanoparticles: Pickering emulsions. Coll. Surf. A Physicochem. Eng. Asp. 2013;439:23–34. https://doi.org/10.1016/j.colsurfa.2013.02.054.